Journal of South American Earth Sciences 59 (2015) 1–12

Contents lists available at ScienceDirect

Journal of South American Earth Sciences

journal homepage: www.elsevier.com/locate/jsames

Magnetotelluric characterization through the Ambargasta-Sumampa Range: The connection between the northern and southern trace of the Río de La Plata Craton – Pampean Terrane tectonic boundary

V. Gisel Peri*, Hernan Barcelona, M. Cristina Pomposiello, Alicia Favetto

Instituto de Geocronología y Geología Isotópica, Pabellón INGEIS, Universidad de Buenos Aires, Consejo Nacional de Investigaciones Científicas y Técnicas, Ciudad Universitaria, C1428EHA Ciudad de Buenos Aires, Argentina

A R T I C L E I N F O

Article history:
Received 12 July 2014
Accepted 23 January 2015
Available online 3 February 2015

Keywords:
Ambargasta-Sumampa Range
Chaco-Pampean Plain
Río de La Plata Craton
Pampean Terrane
Transbrasiliano Lineament
Magnetotelluric

A B S T R A C T

The South American Platform was part of the Western Gondwana, a collage of plates of different ages assembled in late Neoproterozoic to Cambrian times. The Transbrasiliano Lineament, a continental shear belt that transversely intersects this platform from NE to SW, has its southern expression in the tectonic boundary between the Río de La Plata Craton and the Pampean Terrane. Magnetotelluric long-period data in a W–E profile (29°30′ S) that crosses the Ambargasta-Sumampa Range and the Chaco-Pampean Plain were obtained to connect information of this mostly inferred tectonic boundary. A 2-D inversion model shows the Chacoparanense basin, Río Dulce lineament, Ambargasta-Sumampa Range and Salina de Ambargasta in the upper crust. At mid-to-lower crust and 40 km to the east of the Ambargasta-Sumampa Range, a discontinuity (500–2000 Ω m) of 20-km-wide separates two highly resistive blocks, the Río de La Plata Craton (6000–20,000 Ω m) in the east, and the Pampean Terrane (5000–20,000 Ω m) in the west. This discontinuity represents the tectonic boundary between both cratons and could be explained by the presence of graphite. The geometry of the Pampean Terrane suggests an east-dipping paleo-subduction. Our results are consistent with gravimetric and seismicity data of the study area. A more conductive feature beneath the range and the tectonic boundary was associated with the NE–SW dextral transpressive system evidenced by the mylonitic belts exposed in the Eastern Pampean Ranges. This belt represents a conjugate of the mega-shear Transbrasiliano Lineament and could be explained by fluid–rock interaction by shearing during hundreds of years. The eastern border of the Ambargasta-Sumampa Range extends the trace of the Transbrasiliano Lineament. The electrical Moho depth (40 km to the west and 35 km to the east) was identified by a high electrical contrast between the crust and upper mantle. The upper mantle shows a resistive structure beneath the Río de La Plata Craton that could have been originated by stationary delamination by the presence of hydrated lithosphere.

1. Introduction

The South American Platform (Fig. 1a) is constituted by a collage of plates of different ages that were assembled to form Western Gondwana (Cordani et al., 2003, 2013a,b; Tohver et al., 2012; Trindade et al., 2006, among others). The convergence of those continental blocks (~650 My) was along the Transbrasiliano-Kandi mega-shear, a collisional suture (Cordani et al., 2013a). This shear zone, the largest on Earth (Attoh and Brown, 2008), with 6000 Km along South America (Schobbenhaus, 1975) and Africa (Caby, 1989), crosses through many of the Brasiliano-Pan African belts with Neoproterozoic sutures (Cordani et al., 2013a,b). In South America, the Transbrasiliano Lineament (TB) intersects the entire platform from NE to SW (Fig. 1), extending until Argentina along the tectonic boundary between the Paleoproterozoic Río de La Plata Craton (RPC) and the Neoproterozoic-Cambrian (*s.l.*) Pampean Terrane (PT) (Fig. 1b) (Ramos et al., 2010; Rapela et al., 2007). This tectonic boundary is masked by the wide plain developed in the Andean

* Corresponding author. Tel.: +54 011 47833021; fax: +54 011 47833024.
E-mail addresses: gisel@ingeis.uba.ar, gisel_peri@yahoo.com.ar (V.G. Peri), h.lidenbrock@gmail.com (H. Barcelona), cpomposi@ingeis.uba.ar (M.C. Pomposiello), favetto@ingeis.uba.ar (A. Favetto).

http://dx.doi.org/10.1016/j.jsames.2015.01.003
0895-9811/

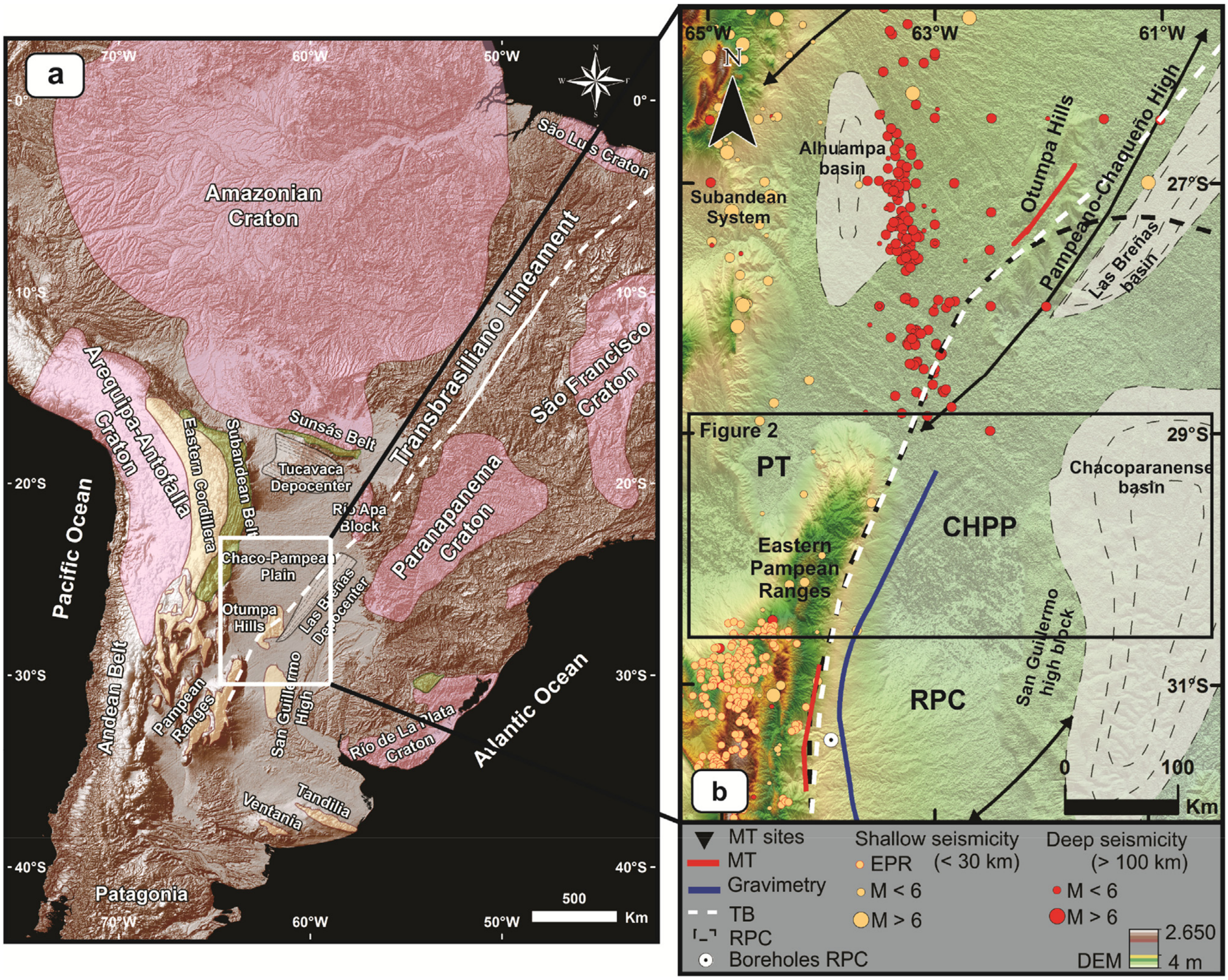

Fig. 1. Geotectonic and geophysical setting. 2-column. a) The main geotectonic features of the South American Platform. b) A detailed map of the study area based on a Digital Elevation Model (DEM), with geotectonic features (PT: Pampean Terrane; RPC: Río de La Plata Craton; CHPP: Chaco-Pampean Plain; TB: Transbrasiliano Lineament), the limit proposed for the RPC (black: Rapela et al., 2011) and those indicated by gravimetry (Ramé and Miró, 2011) and the inferred Transbrasiliano Lineament (TB) (Ramos et al., 2010) is shown. Seismicity (M: magnitude; EPR: seismicity of the Eastern Pampean Ranges represented by yellow circles with red boundary from Richardson et al. (2012)), previous magnetotelluric (MT) data (Favetto et al., 2008; Peri et al., 2013) and the MT sites are also plotted. The rectangle shows the area of Fig. 2. (For interpretation of the references to colour in this figure legend, the reader is referred to the web version of this article.)

foreland and is mostly inferred by geophysical data (Álvarez et al., 2012; Chernicoff and Zapettini, 2004; Ramé and Miró, 2011; Favetto et al., 2008; Peri et al., 2013). Also, several tectonic evolution models are still under debate and essentially imply either east- or west-dipping subduction and a later collision event between the crustal fragments (Ramos, 1988; Ramos et al., 2014; Rapela et al., 1998, 2007; Schwartz and Gromet, 2004; Simpson et al., 2003, among others).

In the present work, we report the results of a MT survey with long-period instruments in a W–E profile located at 29°30′ S and 61°–65° W that crosses the Ambargasta-Sumampa Range (ASR) and the Chaco-Pampean Plain (CHPP) (Fig. 2). We consider it a key localization to connect the northern and southern information of the tectonic boundary between the RPC and the PT. The MT method is an effective and complementary technique to determine lithospheric structures (Bologna et al., 2013; Gowan et al., 2009; Peri et al., 2013; Wannamaker et al., 2008). The MT data obtained were processed to obtain geoelectric strikes and distortion parameters. We also developed a 2-D inversion model that provided the distribution of the measured electrical resistivity of the Earth's subsurface and characterized the lithospheric structure. Finally, we analyze the results with the geotectonic and geophysical context and discuss the possible origins of the electrical configuration.

2. Geological setting

The amalgamation of Western Gondwana developed the Brasiliano-Pan African orogenic belts that closed the Goiás-Pharusian Ocean (650–600 My) and the Transbrasiliano-Kadi mega-shear zone in South America and Africa (Cordani et al., 2003, 2013a, b; Tohver et al., 2012; Trindade et al., 2006, among others). In West Africa, the latter crosses along the Hoggar 4°50′-Kandi shear system (Caby, 1989; Trompette, 1994; Fairhead and Maus, 2003; Santos et al., 2008, among others). In South America, the TB (Schobbenhaus, 1975) transversely intersects the entire platform from NE to SW, from northeast Brazil down to Paraguay and Argentina (Fig. 1a). This mega-shear is active after the closure of the Goiás-Pharusian Ocean, using weak lithospheric collision zones that may involve the entire lithosphere with broad ductile shear zones and many parallel sets of faults (Cordani et al., 2013a, b). To the south of Brazil, the TB was detected by gravimetry in the Paraná basement, crossing the Paraguay Belt (Mantovani and Brito Neves,

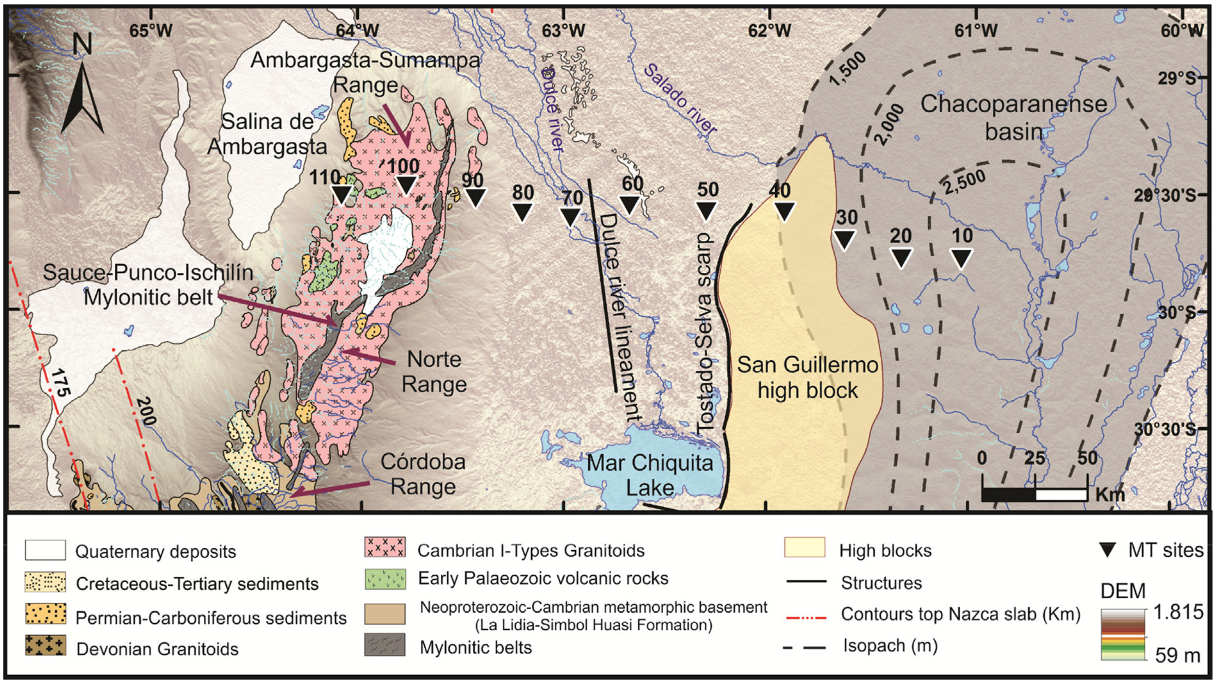

Fig. 2. Geological map. 2-column. A detailed geologic map of the study area (based on Brunetto et al., 2010; Chebli et al., 1999; Iannizzotto et al., 2013; Martino, 2003; Miró and Saap, 2001; Ramos et al., 2010) with the MT sites is shown.

2005). The TB continues in the depocenters Pilar in Paraguay (Wiens, 1985) and Las Breñas in Argentina (Pezzi and Mozetic, 1989), both depocenters with more than 6000 m-thick. Extensional tectonics is evidenced in late Ediacaran times along the northern TB by those depocenters and some intrusion in Goiás, Brazil, of non-deformed potassic granitic bodies (Pimentel et al., 1996) while compressional tectonics is evidenced along the southern TB to the east of the Eastern Pampean Ranges (EPR).

The EPR are part (Fig. 1b) of the broken foreland called the Pampean Ranges (Jordan and Allmendinger, 1986; Ramos et al., 2002) developed by the Pampean flat-slab subduction segment of the central Andes (Alvarado and Ramos, 2011; Anderson et al., 2007; Cahill and Isacks, 1992; Gutscher et al., 2000; among others). Eastward of the EPR, beneath the large CHPP (Chebli et al., 1999), the basement is known by a few boreholes (Fig. 1b) in the Córdoba province, which is constituted by Paleoproterozoic rocks of the RPC (~2–2.3 Gy; Rapela et al., 2007). Meanwhile, the northernmost part of the EPR is constituted by the ASR (Figs. 1 and 2). The North-Ambargasta Range batholith (NARB) represents the Precambrian–Cambrian magmatic arch and is the predominant geological unit. The NARB was emplaced in Late Proterozoic–Early Cambrian host low-grade metamorphic rocks of the La Lidia-Simbol Huasi Formation (Lucero Michaut, 1979; Miró and Saap, 2001; von Gosen and Prozzi, 2010), which has been correlated with the Puncoviscana Formation (*s.l.*) of NW Argentina (von Gosen and Prozzi, 2010), extending the Pampean belt to the north. The NARB constitutes an igneous complex dominated by calc-alkaline I-type granodiorite and monzogranite (Lira et al., 1997) emplaced during Upper Precambrian to Cambrian times (Gromet et al., 2005; Koukharsky et al., 1999; Millone et al., 2003; Rapela et al., 1998; Sims et al., 1998).

An 10 km wide and 70 km long mylonitic strip derived from monzogranite outcrops in the ASR eastern boundary (Fig. 2) in N–S trending and turns SW in the south (Miró and Saap, 2001). This mylonite is poorly known but it is possibly connected to mylonitic strips in Norte Range (von Gosen and Prozzi, 2010) and Córdoba Ranges (Martino, 2003), which register two-stage compressive deformational history during the Early Cambrian (Fig. 2). The mylonitic strip nearest the study area is the Sauce Punco-Ischilín (Iannizzotto et al., 2013), 50 km to the south in the Norte Range with N30° azimuth (Miró et al., 1999; Martino, 2003). From west to east, this strip is essentially constituted by micaceous proto-mylonites, mylonites and ultramylonites derived from pegmatites, rhyodacites to dacites and granitoids which show dextral movement. A compressive deformation D1 at 537 ± 4 My (Iannizzotto et al., 2013) of regional N–S to NE–SW trend with dextral component was identified (von Gosen and Prozzi, 2010) and left pre- or syn-mylonitic plutons of the NARB. A dextral shear deformation D2 developed major mylonitic belts as Sauce Punco-Ischilín (von Gosen and Prozzi, 2010; Iannizzotto et al., 2013) and displaced the Pampean belt relative to the eastern RPC between 537 ± 4 My and 530 ± 4 My (Iannizzotto et al., 2013). A final post-collisional and extensional event was developed in the NARB during the Early Ordovician (ca. 490 My), recorded by the small volcanic and subvolcanic bodies and dykes (Correa, 2003; Leal et al., 2003; O'Leary et al., 2009; Millone, 2004; Rapela et al., 1991).

Three tectonic evolution models of the EPR are still under debate (Ramos et al., 2014). Two of the models imply a collision of an active oceanic ridge, starting with an east-dipping subduction: 1) against the accretion prism of the RPC (Gromet and Simpson, 2000; Schwartz et al. 2008) and 2) against the Kalahari craton, with posterior displacement by a dextral transform fault to the current position and a final collision of the Western Pampean Ranges against the EPR (Rapela et al., 2007). The third model implies a collision of an island arc against the RPC with west-dipping subduction and a final collision of the PT against the amalgamated margin with east-dipping subduction (Escayola et al., 2007, 2011; Ramos et al., 2010). Finally, transtension and transcurrent deformation have occurred along the TB and tectonic reactivations with seismic activity continue until the present (Cordani et al., 2013a,b).

3. Brittle deformation

Several morphostructures characterize the area (Figs. 1 and 2): 1) a depression occupied by the Mar Chiquita Lake, a natural highly saline impoundment; 2) the N–S Dulce River lineament, a probably active structure located north of the Mar Chiquita Lake within the depression area (Casa et al., 2011); 3) the Salina de Ambargasta (Zanor et al., 2012), which occupies a large tectonic depression namely the Saliniana basin (Álvarez et al., 1990), westward of ASR; 4) the San Guillermo high block, which appears to the east (Kröhling and Iriondo, 2003) and was uplifted by faulting reactivation (Brunetto et al., 2010); 5) the N–S Tostado–Selva fault (Pasotti and Castellanos, 1963), the eastern boundary of the Mar Chiquita Lake; and 6) the Chacoparanense depocenter, located to the east of the San Guillermo high block, with 5000 m-thick (Chebli et al., 1999).

4. Geophysical setting

The tectonic boundary between the RPC and the PT was identified by MT data (Fig. 1b) at the limit between the EPR and the CHPP at 32° S (Favetto et al., 2008). Northward, we have reported this boundary at 27° S by a conductive discontinuity between the highly resistive cratons (Peri et al., 2013) (Fig. 1b). Gravimetric profiles have defined this tectonic boundary (Ramé and Miró, 2011) as a 20-km-wide tectonic sheep (Fig. 1b). These results are consistent with an older gravimetric anomaly reported in the Córdoba Ranges (Miranda and Introcaso, 1996) that has been correlated to the same tectonic boundary (Escayola et al., 2007; Ramos, 1988). Moreover, crustal seismic activity is manifested in a horizontal zone between 15 and 25 km depth and active structures including a prominent west-dipping structure beneath the Pampean Ranges and a vertical structure along its eastern margin were reported (Richardson et al., 2012). Some focal mechanism solutions indicate shortening along structures and prove that the EPR are actively deforming in response to compression from the convergent margin. Also, the Moho depth was recorded between 27 and 37 km (Alvarado et al., 2005), of about 35 km beneath the EPR (Gans et al., 2011) and about 38 and 35 km from west to east beneath the Córdoba Ranges (Perarnau et al., 2012; Gans et al., 2011). In the RPC, several authors recorded a Moho depth around 30–40 km (Peri et al., 2013; Sabbione and Rosa, 2009; Sakaguchi et al., 2003).

5. Magnetotelluric method

The MT method provides images of the distribution of electrical conductivity within the Earth. An MT sounding simultaneously measures the time-varying electric and magnetic fields. Variations in the magnetic field induce secondary electric and magnetic fields, which are not independent. MT measurements record the vertical and horizontal components of the magnetic field (Hx, Hy, Hz) and only the horizontal components of the electric field (Ex, Ey), where x and y are orthogonal horizontal directions and z is the vertical direction. By means of the Fourier transform, we converted the time-series obtained into the frequency domain, where the horizontal field components are related by the complex 2 × 2 MT impedance tensor Z (Kaufman and Keller, 1981; Simpson and Bahr, 2005; Vozzoff, 1972):

$$E_x = Z_{xx} H_x + Z_{xy} H_y$$
$$E_y = Z_{yx} H_x + Z_{yy} H_y$$

where Z depends on the subsurface conductivity. This calculation of the frequency provides the electrical structure of the Earth's subsurface. The components of Z allow us to define the apparent resistivity (ρ) and the phase (φ) for each period:

$$\rho_{ij}(\omega) = \frac{1}{\omega\mu}\left|Z_{ij}(\omega)\right|^2(\Omega.m) \qquad \phi_{ij}(\omega) = \frac{1}{\omega\mu}\frac{\mathrm{Im}(Z_{ij}(\omega))}{\mathrm{Re}(Z_{ij}(\omega))}$$

where μ is the magnetic permeability of free space.

The conductivity varies with depth for a 1-D layered Earth, the diagonal components of Z are zero, and the off-diagonal elements are equal in magnitude but have opposite signs. In a 2-D medium, the conductivity parallel to the structural strike is constant and varies with both the direction perpendicular to the strike and the depth, the diagonal components of Z are equal to zero, and the off-diagonal elements differ in magnitude and have opposite signs. A tensor rotation allows us to find two orthogonal directions in which the diagonal components of Z are close to zero. One of these directions coincides with the geological structure and is called the geoelectric strike. In this case, data can be separated into two independent modes with electrical current flowing parallel and perpendicular to the strike direction (transverse electric and magnetic polarizations) (Kaufman and Keller, 1981; Vozzoff, 1972). It is not always possible to find a geoelectric strike usually due to the presence of distortion, 3-D induction, or both.

6. Data acquisition and processing

MT data were obtained from 11 long-period stations spaced ~30 km apart along a 300 km-long W–E profile at 29°30′ S that crossed the ASR and CHPP (Fig. 2). The electric (Ex, Ey) and magnetic (Hx, Hy, Hz) fields were orthogonally recorded at the surface with axis directions defined as x to the north, y to the east and z down. The electric field was measured with pairs of Pb–$PbCl_2$ electrodes and the magnetic field with a Narod Intelligent Magnetotelluric System, which includes a "fluxgate" type magnetometer and records between 1 and 10,000 s, a period range of interest for regional geodynamic studies. The signal was recorded for 300 h in average. The robust multiple-station MT data processing software algorithm using multivariate statistical methods of Egbert (1997) was applied to the MT time-series data collected to identify and remove coherent and incoherent noise. The data were processed using the Fourier transform, and the impedance was estimated. The components of the MT impedance tensor and two magnetic transfer functions were calculated for logarithmically spaced frequencies using the statistically robust method of Egbert and Booker (1987). Finally, smooth resistivity curves consistent with phases were obtained. The values measured and the values calculated for the final 2-D inversion model were included (see section 8). The pseudosections of apparent resistivity (ρ) and phase (φ) for both polarizations in the measurement coordinates and tipper magnitude for the frequency range of 10^{-4}–10^{-1} Hz are shown in Fig. 3.

7. Dimensionality and distortion

The best geoelectric strike direction and the medium's dimensionality were analyzed. For a local and regional 2-D structure, a rotation of the impedance tensor is needed to determine its principal axes. For more complex structures, with locally anomalous 3-D conductivity, the data are influenced by galvanic distortions or 3-D dimensionality effects. The distortion is almost entirely confined to the electric field. In this work, the dimensionality and distorted parameters and the best geoelectric strike direction were determined by the tensor decomposition technique (McNeice and Jones, 2001) based on the Groom-Bailey decomposition code (1989).

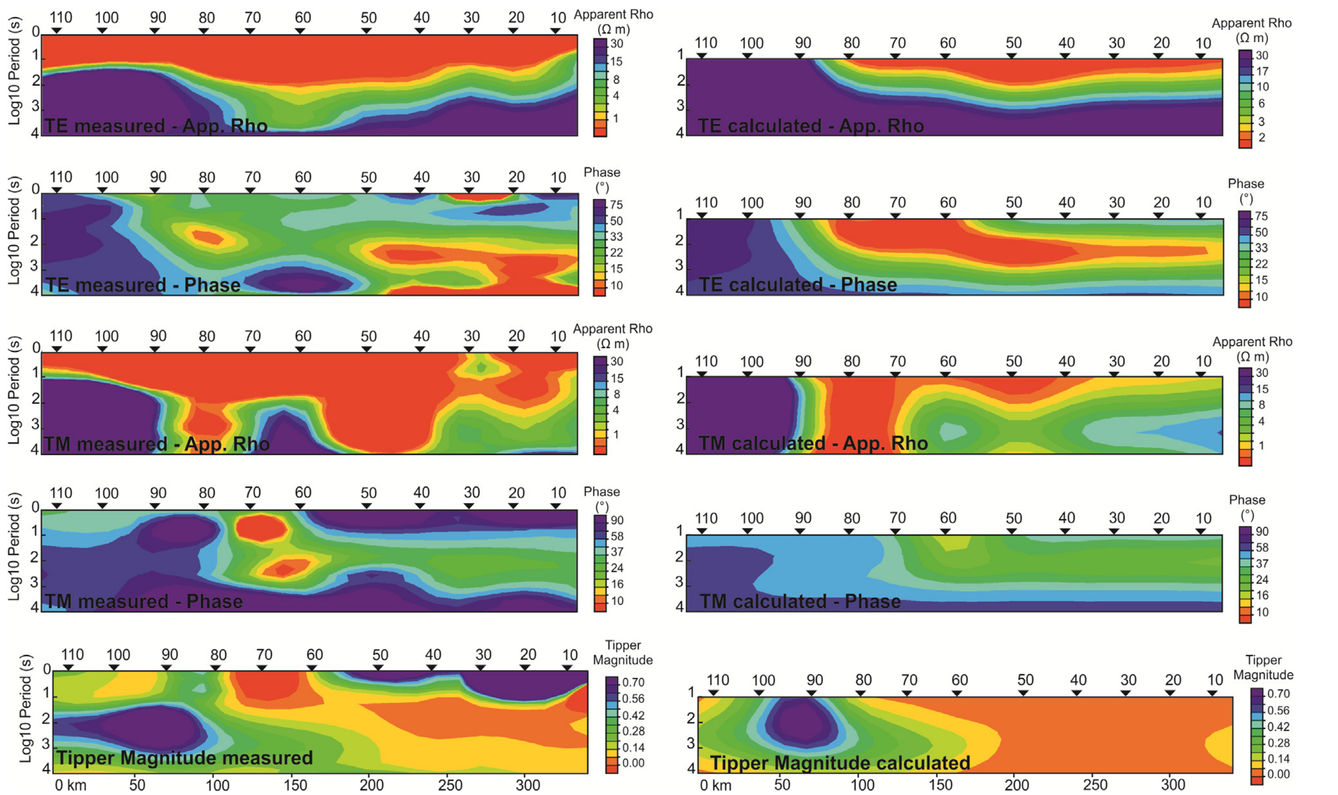

Fig. 3. Pseudosections. 2-column. MT data (measured) and model response (calculated) for the final 2-D inversion model's pseudosections of the apparent resistivity (Apparent Rho, Ω m) and phase (Phase, °) for transverse electrical polarization (TE), transverse magnetic polarization (TM) and tipper magnitude. The pseudosections for the calculated data show periods from 10 to 10,000 s, which is the range used in the 2-D inversion.

Tensor decomposition methods can be applied to remove effects caused by near-surface inhomogeneities and to recover parameters of the magnetotelluric impedance tensor (twist, shear and skew or anisotropy tensor) that partially describes the distortion effects.

The regional strikes were calculated by the Strike code of McNeice and Jones (2001). Single-site multi-frequency analysis was carried out without any constraint for the four period ranges and for the average of each site to analyze the responses at different scales (Fig. 4). Also, the strike was fixed for different angles and the misfit for each was analyzed to obtain the mean strike direction with the best fit for all MT sites. The misfit values for each strike selected are shown in the line diagrams in Fig. 4. The strike value corresponding with the lowest misfits was N5°E. Finally, each MT site was rotated by the selected strike to obtain the final rho and phase curves. For the period range between 1 and 10 s the regional strike has showed an average of N36°E, between 10 and 100 s indicated a strike of N26°W and for periods between 100 and 1000 s and 1000 and 10,000 s the strike was N15°W and N10°E, respectively (Fig. 4). The average strike for all periods (1–10,000 s) of all the MT sites was N2°E (Fig. 4).

Twist and shear distortion parameters were less than ±5°, whereas a few were greater than ±5°. Finally, a common geoelectric strike of N5°E was assumed based on the regional geological structure and all the data were rotated by 5° into the profile direction. Although the distortion was weak, it was taken into account in the 2-D inversion.

8. Geological constraints and 2-D inversion model

The initial model was developed over a mesh with geological constraints that allowed us to obtain a more realistic result and helped us to overcome the non-uniqueness problem (Fig. 5a and b). The 2-D inversion of the MT data was carried out with the non-linear conjugate gradient algorithm of Rodi and Mackie (2001) available in the WinGLink software. Each MT station was centered in columns with a regular arrangement in the profile and the rows were added at depths with a logarithmic spacing. The outer 4-km layer was represented by a sedimentary cover with a resistivity of 50 Ω m. The ocean was characterized in the west side of the profile as being 5 km thick and having a resistivity of 0.3 Ω m. The Chacoparenense basin, which is located on the east side of the profile, was characterized with a resistivity of 3 Ω m, with a maximum depth of 5 km that decreased to the profile center. The Mar Chiquita depression was represented with a 50-m-thick layer with a resistivity of 1 Ω m. The entire crust is around 40 km thick, was exposed at the ASR located on the west side of the profile, and was characterized with a resistivity of 10,000 Ω m. The remainder of the lithosphere was assigned a resistivity of 1000 Ω m. Below a depth of 200 km, the asthenosphere was represented with a resistivity of 10 Ω m.

The inversion parameters were modified to analyze different results. The roughness model was minimized through the iterative algorithm toward a pre-established misfit. Several inversions were performed to generate the most reliable model. The period range between 10 and 10,000 s was used. The final model (Fig. 5c and d) had the most reliable features expected by the geological data and the previously calculated parameters. The smoothness parameter Ʈ had a value of 1 in the final model. The resistivity error floors were 10%, and the phase error floors were 2.9°. Thus, a higher weight was assigned to the phases to overcome the static shift problem. In addition, a value of 0.05 was selected for the tipper and horizontal magnetic data. The resistivity values were limited to 20,000 Ω m to avoid extreme values. The final NRMS for each MT site is shown in Fig. 5. This model presented a

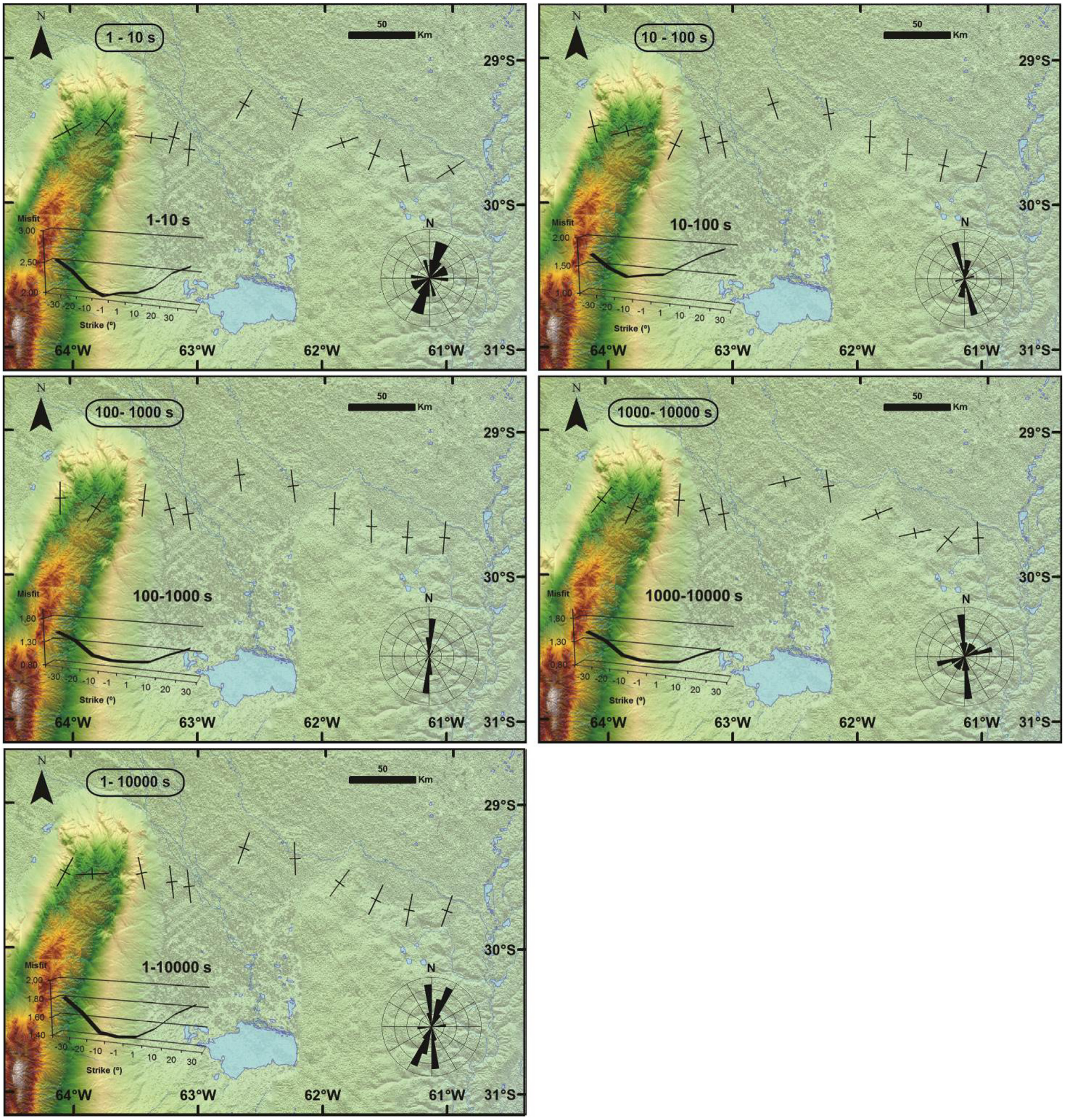

Fig. 4. Geoelectric strikes. 2-column. Regional geoelectric strikes determined for four period ranges (1–10 s, 10–100 s, 100–1000 and 1000–10,000 s) and for the average strike of each site. The rose diagram for each site and the misfit vs. the strike fixed for each period range are also shown.

good inversion misfit with an NRMS of 1.985. The features observed were consistent in all the tests. The pseudosections of the apparent resistivity (ρ) and phase (φ) calculated for both polarizations and tipper magnitude for the period range of 10 – 10,000 s are shown in Fig. 3.

9. Geoelectric model

The final geoelectric model (Fig. 6) shows a sedimentary cover characterized by a 5-km-thick upper layer A with resistivity values between 15 and 75 Ω m and a more conductive layer B with resistivity values of <5 Ω m. At the eastern extreme of the profile in the Chacoparanense depocenter, layer B is well characterized and reaches a maximum of 3200 km thick at around site 10. Layer B appears again around site 70 along 40 km width and between 1300 and 3000 m depth as well as at the western extreme of the profile along 30 km width and between 1000 and 2500 m depth. The mid-to-lower crust showed high resistivities and reached a maximum depth of 40 km to the west and revealed two highly resistive features: one in the east (C), with resistivity values between 6000 and 20,000 Ω m, and the other in the west (D), with resistivities between 5000 and 20,000 Ω m. Both features show a decrease in resistivity to its boundaries (~1000 Ω m). The diffuse boundaries are due to the 2-D inversion carried out with the non-linear conjugate gradient algorithm (Rodi and Mackie, 2001) so the net boundaries are inferred.

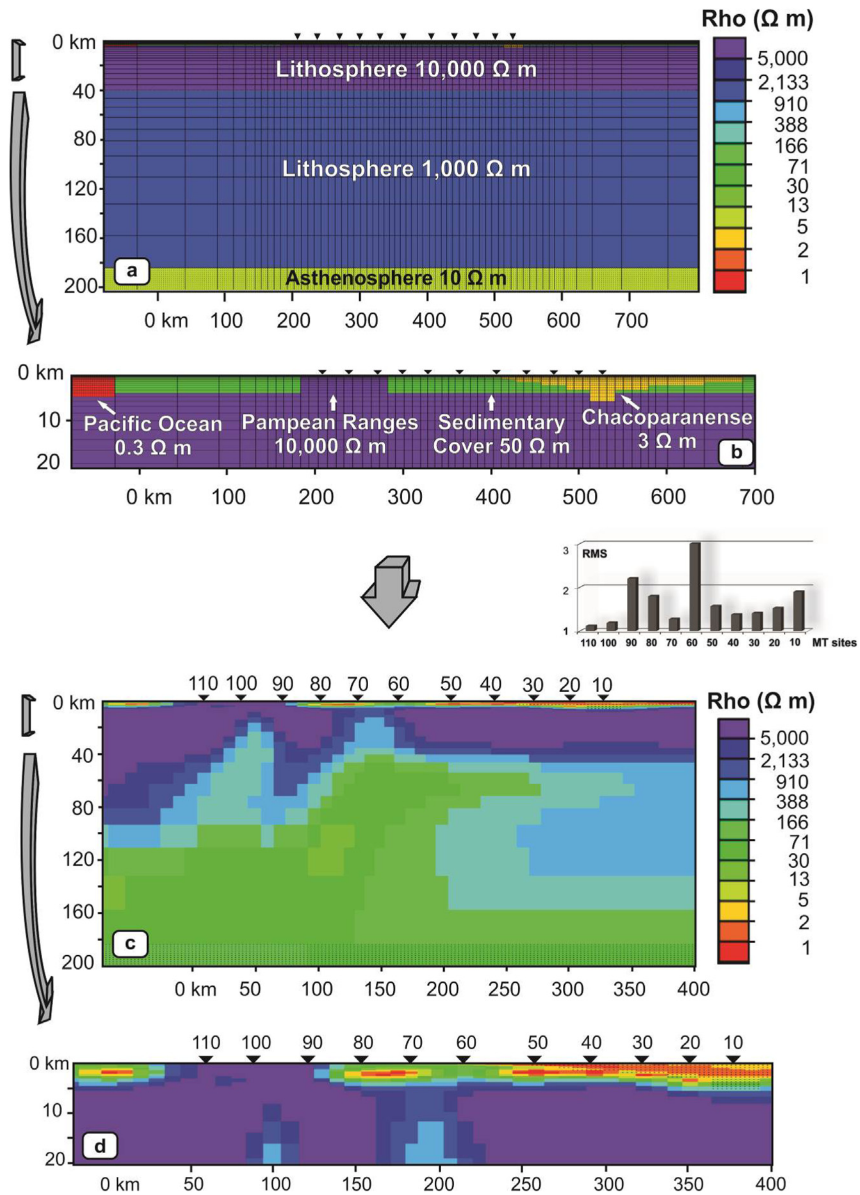

Fig. 5. 2-D inversion model. 2-column. a) The initial mesh for the 2-D inversion model with geological constraints. b) A detail of 20 km-thick with the known shallow features. c) The final 2-D inversion model obtained at depths of 200 km and the frequency distribution of the NRMSs obtained for each MT site are shown. d) A detail of the final 2-D inversion model obtained at 20 km depth.

Block C develops between 3.8 and 35 km depth and maintains a horizontal disposition while Block D develops between 4 and 40 km depth and shows a different geometry. Also, between sites 90 and 110, Block D reaches the surface around 70 km width, coinciding with the ASR and between the sites 90 and 70 shows a very gentle east dip. Block C has a root between 35 and 45 km, with resistivities between 3200 and 1600 Ω m that decrease with depth. A similar root (C_2) with resistivity around 800 Ω m appears between 80 and 100 km depth. Block D is a discontinuous feature since it shows a conductive area E of 200 to 4000 Ω m below sites 90 and 100 between 10 and more than 40 km depth and a variable width between 10 and 25 km that expands in depth. A more conductive 20-km-wide discontinuity F with resistivities of 400 to 2000 Ω m is located between the resistive blocks between 4 and 35 km depth. This feature was observed in all the inverted models. Finally, a very conductive feature G is observed at upper mantle depth between 40 and 80 km, which extends along 150 km width at the center of the profile beneath feature F with resistivities between 20 and 70 Ω m.

10. Discussion

10.1. Geological approach integrated to gravimetric and seismicity data

The shallowest features at upper crust levels reflect the Chacoparanense depocenter in the east of the profile. The very conductive layer B fills this basin, which reaches around 3200 m depth (Figs. 6 and 7). This layer B is interrupted by a more resistive narrow area with a vertical disposition between sites 60 and 70 just above the deeper discontinuity F, which could represent the Río Dulce Lineament in depth (Fig. 7). To the west of ASR, outside the profile, another conductive area conformed by layer B represents the Salina de Ambargasta with 2500 m depth (Figs. 6 and 7).

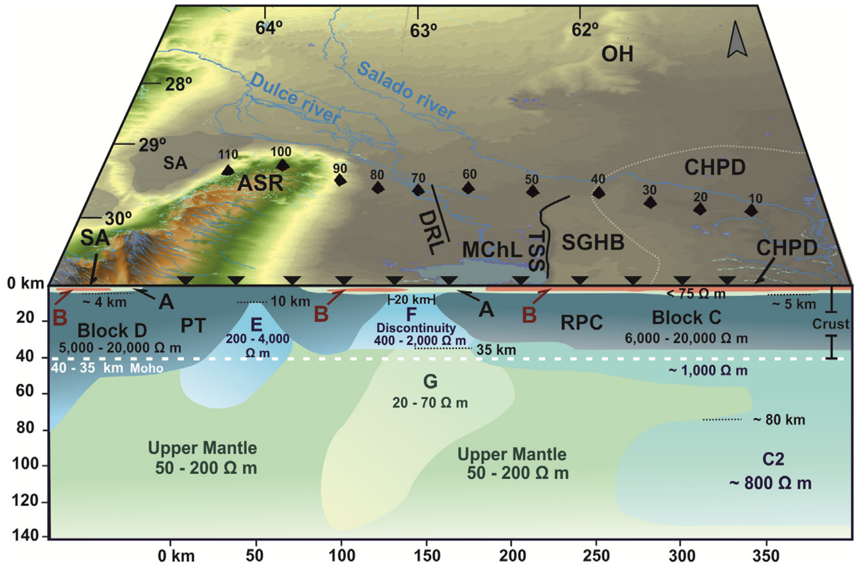

Fig. 6. Geoelectric model. 2-column. The geoelectric interpretation of the 2-D inversion model obtained is shown at a depth of 140 km. The MT sites are shown in black triangles and pyramids. Letters A-G represent the geoelectric features described in the text: A–B: very conductive layers; C–D: highly resistive blocks; E–F: crustal more conductive features; G: upper mantle conductive feature; C_2: upper mantle more resistive feature. Geological references: ASR: Ambargasta-Sumampa Range; CHPD: Chacoparanense depocenter; DRL: Dulce river lineament; MChL: Mar Chiquita Lake; OH: Otumpa hills; PT: Pampean terrane; RPC: Río de La Plata Craton; SA: Salina Ambargasta; SGHB: San Guillermo high block; TSS: Tostado-Selva Scarpment.

When analyzing the entire crust, the presence of the ASR indicates that the western Block D corresponds to the PT and the Paleoproterozoic ages of the eastern basement (see section 2) indicates that the highly resistive Block C corresponds to the RPC (Figs. 6 and 7). Thus, the crustal discontinuity F, located 40 km to the east of the ASR, represents their tectonic boundary, hence the Cambrian suture. Besides, the PT shows a very gentle east dip immediately to the west of the tectonic boundary while the RPC remains horizontal. Similar features are also observed in the northern MT model (Peri et al., 2013) although the PT shows a more regular geometry probably because farther of the Pampean oronegy the model is simpler. Both MT models allow us to extend the trace of the Cambrian suture between the PT and the RPC and also agree with an east-dipping paleo-subduction. The gravimetric models of Ramé and Miró (2011) in the ASR show a high gravimetric gradient in the tectonic boundary between the cratons. This gradient is spatially very close to our more conductive zone F and these authors have defined it as a

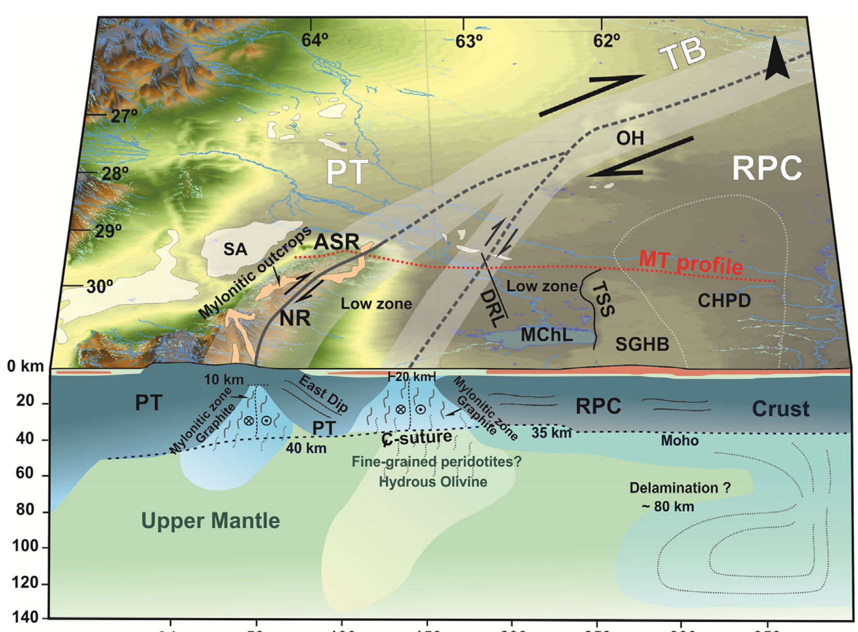

Fig. 7. Geodynamic model. 2-column. The block diagram shows the geodynamic interpretation of the study area. The MT profile is almost 100 km to the north of the vertical section. The PT has a very gentle east dip while the RPC remains horizontal. The Cambrian suture (C-suture) between both cratons is observed 40 km to the east of ASR. The mylonitic zones are associated with the more conductive features and the TB. Geological references: ASR: Ambargasta-Sumampa Range; CHPD: Chacoparanense depocenter; DRL: Dulce river lineament; MChL: Mar Chiquita Lake; NR: Norte Range; OH: Otumpa hills; PT: Pampean terrane; RPC: Río de La Plata Craton; SA: Salina Ambargasta; SGHB: San Guillermo high block; TB: Transbrasiliano Lineament; TSS: Tostado-Selva Scarpment.

tectonic sheet. Moreover, this feature is around 20 km wide for both data.

Another more conductive feature E of the mid-to-lower crust with a more or less vertical shape is observed in Block D below the ASR (Figs. 6 and 7) which coincides with an eastern 10-km-wide mylonitization strip. We suggest a possible connection of the deformed granite with the southern Sauce-Punco-Ischilín mylonitic belt, which shows a dextral kinematics. So, we propose that this more conductive feature jointly with the discontinuity between the cratons F could correspond to a shear dextral belt system of the TB and extends in the entire crust (Fig. 7). Although the mylonitic strip kinematics in ASR is unknown, it could represent a conjugate of the main TB mega-shear. Finally, E has a top around 10 km depth (Figs. 6 and 7) wherein an intra-crustal seismic discontinuity was found at south (Perarnau et al., 2012). Probably, the limit upper-lower crust lies between 10 and 20 km.

The MT model shows a Moho depth very similar to that shown by the seismic data of the south (Perarnau et al., 2012). The eastern side of the MT model shows 35 km depth while the western side reaches 40 km depth (Figs. 6 and 7). The seismic Moho was defined by a large contrast in seismic velocities with a consistent signal, between the crust and the upper mantle. This depth has showed a correspondence with the large electrical contrast of highly resistive and conductive values of the crust and the upper mantle, respectively. There is a relation between the marked contrast in the electrical MT values and the seismic signal to define the electrical and seismic Moho, respectively. So, our data provide continuity to the seismic crustal thickness in the northernmost part of the EPR.

Another interesting relation is that observed with the EPR seismicity described by Richardson et al. (2012) southward of the study area. These authors found active structures such as west-dipping structure beneath the EPR and a vertical structure along the eastern margin. We associated the west-dipping structure with E and the vertical structure in the eastern margin with F. On the other hand, the seismicity and brittle behavior was constrained to the upper ~25 km of the crust (Perarnau et al., 2012) as well as an aseismic ductile shear zone below a mid-crustal discontinuity around 22–27 km. In agreement, the MT model shows a more conductive and a probably more ductile behavior beneath those depths (E and F) (Fig. 7).

10.2. Electrical conduction mechanisms in the crust

The highly resistive blocks of the mid-to-lower crustal observed in the MT model are consistent with old and stable regions which typically are between 1000 and 10,000 Ω m (Chave and Jones, 2012; Jones, 2013). The more conductive areas E and F at lower crust depths can be explained by the presence of good conductors with interconnected grain-boundary arrangements, such as saline fluids, sulfides, graphite films, and metallic and partial melt material (Brown, 1994; Chouteau et al., 1997; Jones, 1992; Jones et al., 2005; Livelybrooks et al., 1996; Selway, 2012; Türkoğlu et al., 2008). The old subduction led us to conjecture that a preferential alignment at least 0.02% (Mareschal et al., 1992) of graphite films along grain boundaries could have originated the more conductive values at lower crust depths. The graphite may be biogenic, *e.g.* derived from the underthrusting of organic graphite-bearing metasedimentary rocks, or inorganic precipitated from CO_2-rich fluids derived from the mantle as a product of CO_2 degassing (Brown, 1994).

Graphitic horizons are common tectonic markers of old orogenies and deep crustal deformation and hence can reveal paleosuture zones (Boerner et al., 1996). The low temperatures of the study area suggest that the graphite was formed by strain energy of a transpressive regime and the shear belts exposed in this area support this idea. Additionally, the presence of inorganic graphite or interconnected sulfide deposits or other conductive minerals that are concentrated in reduced regions of intense fluid–rock interaction, such as shear zones (Selway, 2012), could decrease the resistivity. So, at lower crust depths, the graphite indicates an old subduction zone and must be related to the Neoproterozoic-Cambrian convergent tectonic processes of the RPC and the PT (Fig. 7), whereas at upper crust depths the fluid–rock interaction of a mega-shear zone dominated and must be related to the TB.

10.3. Electrical conduction mechanisms in the mantle

At upper mantle depths, Block C shows a root (C_2) with resistivities of 800 Ω m (Fig. 6). This feature has also been identified in the northern MT profile at 27° S (Peri et al., 2013). Next to this feature, a highly conductive zone G is observed between the cratons (Fig. 6). Thick lithospheric roots beneath cratons exhibit large variations (Artemieva and Mooney, 2002; Eaton et al., 2009). Eaton et al, (2009) reported a lithosphere-asthenosphere boundary that varies broadly between 150 and 300 km depth, and Proterozoic cratons, such as this case, are usually 150–200 km thick (Jones, 2013). The Block C_2 can be related to delamination of the RPC, which, after a long period of stability, is affected by erosion of its base (Fig. 7). Krystopowicz and Currie (2013) have postulated the retreating and stationary delaminations. They observed that a weak crust less dense than the mantle eclogitized crust leads the entire mantle lithosphere to be delaminated while higher density eclogite helps drive delamination.

Additionally, a hydrated upper mantle and the shortening of this intraplate between 3 and 6 cm/year (Marotta et al., 2013), can favor the delamination processes. The highly conductive zone G could be related to a hydrated lithosphere (Fig. 7) due to the conduction by hydrogen (proton) diffusion in hydrous olivine or other anhydrous minerals (garnet, orthopyroxene, clinopyroxene or plagioclase) (Dai and Karato, 2009; Karato, 1990, 2006; Mookherjee and Karato, 2010; Selway, 2012; Yang et al., 2011, 2012; Yoshino et al., 2008, 2009). A subducted slab introduces hydrogen into the lithosphere and decreases the resistivity (Selway et al., 2014). Moreover, the presence of fine-grained peridotites, which occur in mylonitic zones, may show electrical conductivities up to two orders of magnitude higher than coarser-grained samples (ten Grotenhuis et al., 2004) (Fig. 7). So, we considered that a stationary delamination could explain the presence of Block C_2 below the RPC. The presence of G, which is possibly a hydrated and peridotitic area, supports this idea. The past geological events such as the paleo-subduction and the posterior mega-shear zone strongly influence the electrical resistivities of stable lithospheric regions because they enrich the lithosphere in incompatible elements and hydrogen and grain-boundary graphite films (Selway, 2012). However, further geological evidence is lacking in this area and the mantle processes are still controversial.

11. Conclusions

New MT data provided an electrical characterization of the crust and upper mantle through the ASR and the CHPP (29°30′S – 61°-65° W). The main conclusions follow:

a) Some the following upper crust features were recognized: 1) the Chacoparanense basin, with very conductive fills and 3200 m depth; 2) a more resistive shallow structure possibly linked to the Río Dulce lineament; 3) the ASR, highly resistive and related to the PT; and 4) the Salina de Ambargasta, with a very conductive fill and 2500 m depth.
b) The highly resistive blocks at crustal depths correspond to the RPC (Block C: 6000 to 20,000 Ω m) in the east, and to the

PT (Block D: 5000 to 20,000 Ω m) in the west. Between both blocks, eastward of the ASR, was identified the more conductive feature F (500–2000 Ω m) with 20-km-wide and beneath the ASR, was identified the feature E (200–4000 Ω m).

c) The discontinuity between the cratons could indicate deep deformation of the crust and reveal the location of the paleosuture zone, around 40 km to the east of the ASR, between the PT and the RPC explained by the presence of graphite. A very gentle east-dipping old subduction against the RPC was observed such as in the northern MT model.
d) Although there is a lack of geological evidence in this area, our results are supported by gravimetric data that defined the same tectonic boundary to the east of the ASR.
e) The more conductive features F and E are associated with the NE–SW dextral transpressive system evidenced by the mylonitic belts exposed in the EPR and could be explained by fluid–rock interaction predominantly at upper crust depth, by intense shear during hundreds of millions of years.
f) The mylonitic belt could represent a conjugate of the main TB mega-shear structure, developed during the final stages of the assembly of West Gondwana, in Ediacaran and Cambrian times and active until the present, and is spatially associated with the paleosuture.
g) The new MT data were obtained from a key position to join the scarce geophysical information obtained at north (27° S) and at south in the Córdoba Ranges (32° S) and to improve the inferred trace of tectonic boundary between the PT and the RPC and the TB.
h) We defined an electrical Moho depth by a high contrast between the highly resistive crust and more conductive upper mantle that reaches 40 km to the west and 35 km to the east, according to the southern seismic data. Seismicity data identified a west-dipping structure beneath the ranges and a vertical structure along their eastern margin which are consistent with the more conductive and crustal features of the MT model.
i) The upper mantle depth shows a resistive structure beneath the RPC that could be explained by stationary delamination that commonly occurs in stable regions during long periods of times. A conductive feature immediately to the west of it could indicate a hydrated lithosphere by the presence of hydrated mantle minerals and/or of fine-grained peridotites, both of which can increase conductivity.

Acknowledgments

We acknowledge the Argentine Council for Scientific and Technical Research (CONICET, grant PIPD703, 2011) for providing financial support to improve the logistics. The MT systems were provided by the EMSOC Instrument Facility, which is supported by NSF grants EAR02-36538 and EAR96-16421. We also thank Gabriel Giordanengo (Instituto de Geocronología y Geología Isotópica, INGEIS) for his valuable technical assistance during the surveys. We also thank Dr. Cordani, the anonymous reviewer and the Editors, who have provided suggestions that have improved the manuscript.

References

Alvarado, P., Castro de Machuca, B., Susan Beck, S., 2005. Comparative seismic and petrographic crustal study between the Western and Eastern Sierras Pampeanas region (31°S). Rev. la Asoc. Geol. Argent. 60 (4), 787–796.
Alvarado, P., Ramos, V.A., 2011. Earthquake deformation in the northwestern Sierras Pampeanas of Argentina based on seismic waveform modeling. J. Geodyn. 51, 205–218.
Anderson, M., Alvarado, P., Zandt, G., Beck, S., 2007. Geometry and brittle deformation of the subducting Nazca plate, central Chile and Argentina. Geophys. J. Int. 171 (1), 419–434.
Álvarez, L.A., Fernández Seveso, F., Pérez, M.A., Bolatti, N.D., 1990. Estratigrafía de la Cuenca Saliniana. XI Congreso Geológico Argentino, San Juan. Actas 2, 145–148.
Álvarez, O., Gimenez, M., Braitenberg, C., Folguera, A., 2012. GOCE satellite derived gravity and gravity gradient corrected for topographic effect in the South Central Andes region. Geophys. J. Int. 190 (2), 941–959.
Artemieva, I.M., Mooney, W.D., 2002. On the relations between cratonic lithosphere thickness, plate motions, and basal drag. Tectonophysics 358, 211–231.
Attoh, K., Brown, L.D., 2008. The Neoproterozoic trans-saharan/trans-brasiliano shear zones: suggested Tibetan analogs. Eos Trans. AGU 89 (23) (Joint Assembly Supplement) abstract S51A-04.
Boerner, D.E., Kurtz, R.D., Craven, J.A., 1996. Electrical conductivity and Paleo-Proterozoic foredeeps. J. Geophy. Res. 101 (13), 775–789.
Bologna, M.S., Nunes, H.O., Padilha, A.L., Vitorello, Í., Pádua Marcelo, B., 2013. Anomalous electrical structure in the northwestern Paraná Basin, Brazil, observed with broadband magnetotellurics. J. South Am. Earth Sci. 42, 74–82.
Brown, C., 1994. Tectonic interpretation of regional conductivity anomalies. Surv. Geophys. 15, 123–157.
Brunetto, E., Iriondo, M., Zamboni, L., Gottardi, G., 2010. Quaternary deformation around the Palo Negro area, Pampa Norte, Argentina. J. South Am. Earth Sci. 29, 627–641.
Caby, R., 1989. Precambrian terranes of Benin, Nigeria and northeast Brazil and the late proterozoic south Atlantic fit. Geol. Soc. Am. Special Pap. 230, 145–158.
Cahill, T., Isacks, B., 1992. Seismicity and shape of the subducted Nazca plate. J. Geophys. Res. 97, 17503–17529.
Casa, A., Yamin, M., Wright, E., Costa, C., Coppolecchia, M., Cegarra, M., 2011. Deformaciones Cuaternarias de la República Argentina, Sistema de Información Geográfica. Instituto de Geología y Recursos Minerales. Servicio Geológico Minero Argentino. Publicación N° 171, V 1.0 en formato DVD.
Chave, A.D., Jones, A.G., 2012. The Magnetotelluric Method, Theory and Practice, first ed. United Kingdom, Cambridge.
Chebli, G., Mozetic, M., Rossello, E., Bühler, M., 1999. Cuencas sedimentarias de la llanura Chacopampeana. In: Caminos, R. (Ed.), Geología Argentina, Anales 29(20). Instituto de Geología y Recursos Minerales, Buenos Aires, pp. 627–644.
Chernicoff, C.J., Zappettini, E.O., 2004. Geophysical evidence for terrane boundaries in south-central Argentina. Gondwana Res. 7, 1105–1116.
Chouteau, M., Zhang, P., Dion, D.J., Giroux, B., Morin, R., Krivochieva, S., 1997. Delineating mineralization and imaging the regional structure with magnetotellurics in the region of Chibougamau (Canada). Geophysics 62 (3), 730–748.
Cordani, U.G., D'Agrella-Filho, M.S., Brito Neves, B.B., Trindade, R.I.F., 2003. Tearing up Rodinia: the Neoproterozoic palaeogeography of South American cratonic fragments. Terra Nova 15, 350–359.
Cordani, U.G., Pimentel, M.M., Ganade de Araújo, C.E., Basei, M.A.S., Fuck, R.A., Girardi, V.A.V., 2013a. Was there an Ediacaran Clymene ocean in central south America? Am. J. Sci. 313, 517–539.
Cordani, U.G., Pimentel, M.M., Ganade de Araújo, C.E., Fuck, R.A., 2013b. The significance of the Transbrasiliano-Kandi tectonic corridor for the amalgamation of West Gondwana. Braz. J. Geol. 43 (3), 583–597.
Correa, M.J., 2003. Petrología y edad K/Ar de diques relacionados a la Formación Oncán, sierra de Ambargasta, Santiago del Estero. Rev. la Asoc. Geol. Argent. 58 (4), 664–668.
Dai, L., Karato, S-i, 2009. Electrical conductivity of orthopyroxene: implications for the water content of the asthenosphere. Proc. Jpn. Acad. Ser. B-Phys. Biol. Sci. 85 (10), 466–475.
Eaton, D.W., Darbyshire, F., Evans, R.L., Grütter, H., Jones, A.G., Yuan, X., 2009. The elusive lithosphere–asthenosphere boundary (LAB) beneath cratons. Lithos 109, 1–22.
Egbert, G.D., 1997. Robust multiple-station magnetotelluric data processing. Geophys. J. Int. 130, 475–496.
Egbert, G., Booker, J., 1987. Robust estimation of geomagnetic transfer function estimation. Geophys. J. R. Astro. Soc. 87, 173–194.
Escayola, M.P., Pimentel, M.M., Armstrong, R., 2007. Neoproterozoic backarc basin: sensitive high-resolution ion microprobe U-Pb and Sm-Nd isotopic evidence from the Eastern Pampean ranges, Argentina. Geology 35, 495–498.
Escayola, M.P., van Staal, C.R., Davis, W.J., 2011. The age and tectonic setting of the Puncoviscana Formation in northwestern Argentina: an accretionary complex related to Early Cambrian closure of the Puncoviscana Ocean and accretion of the Arequipa-Antofalla block. J. South Am. Earth Sci. 32 (4), 438–459.
Fairhead, J.D., Maus, S., 2003. CHAMP satellite and terrestrial magnetic data help define the tectonic model for South America and resolve the lingering problem of the pre-break-up fit of the South Atlantic ocean. Lead. Edge 22 (8), 779–783.
Favetto, A., Pomposiello, C., López de Luchi, M., Booker, J., 2008. 2D magnetotelluric interpretation of the crust electrical resistivity across the Pampean terrane - Río de la Plata suture, in central Argentina. Tectonophysics 459, 54–65.
Gans, C., Beck, S., Zandt, G., Gilbert, G., Alvarado, P., Anderson, M., Linkimer, L., 2011. Continental and oceanic crustal structure of the Pampean flat slab region, western Argentina, using receiver function analysis: new high-resolution results. Geophys. J. Int. 186 (1), 45–58.
Gowan, E.J., Ferguson, I.J., Jones, A.G., Craven, J.A., 2009. Geoelectric structure of the northeastern Williston basin and underlying Precambrian lithosphere. Can. J. Earth Sci. 46, 441–464.
Gromet, I.P., Simpson, C., 2000. Cambrian Orogeny in the Sierras Pampeanas, Argentina: Ridge Subduction or Continental Collision? Geological Society of America. Abstract with Programs 32, A–505. Boston.

Gromet, L.P., Otamendi, J.E., Miró, R.C., Demichelis, A.H., Schwartz, J.J., Tibaldi, A.M., 2005. The Pampean Orogeny: Ridge Subduction or Continental Collision? Gondwana 12. Academia Nacional de Ciencias, Mendoza, Argentina. Abstract 183.

Groom, R.W., Bailey, R.C., 1989. Decomposition of magnetotelluric impedance tensor in the presence of local three-dimensional galvanic distortion. J. Geophys. Res. 94, 1913–1925.

Gutscher, M.A., Spakman, W., Bijwaard, H., Engdahl, E.R., 2000. Geodynamics of flat subduction: seismicity and tomographic constraints from the Andean margin. Tectonics 19, 814–833.

Iannizzotto, N.F., Rapela, C.W., Baldo, E.G.A., Galindo, C., Fanning, C.M., Pankhurst, R.J., 2013. The sierra Norte-Ambargasta batholith: late Ediacaran-early Cambrian magmatism associated with Pampean transpressional tectonics. J. South Am. Earth Sci. 42, 127–143.

Jones, A.G., 1992. Electrical conductivity of the continental lower crust. In: Fountain, D.M., Arculus, R.J., Kay, R.W. (Eds.), Continental Lower Crust. Elsevier, Amsterdam, pp. 81–143.

Jones, A.G., 2013. Imaging and observing the electrical Moho. Tectonophysics 609, 423–436.

Jones, A.G., Ledo, J., Ferguson, I.J., Farquharson, C., Garcia, X., Grant, N., McNeice, G., Roberts, B., Spratt, J., Wennberg, G., Wolynec, L., Wu, X.H., 2005. The electrical resistivity structure of archean to tertiary lithosphere along 3200 km of SNORCLE profiles, northwestern Canada. Can. J. Earth Sci. 42, 1257–1275.

Jordan, T.A., Allmendinger, R.W., 1986. The Sierras Pampeanas of Argentina: a modern analogue of rocky mountain foreland deformation. Am. J. Sci. 286, 737–764.

Karato, S-i, 1990. The role of hydrogen in the electrical-conductivity of the upper mantle. Nature 347 (6290), 272–273.

Karato, S-i, 2006. Remote sensing of hydrogen in Earth's mantle. In: Keppler, H.S.J.R. (Ed.), Water in Nominally Anhydrous Minerals, Reviews in Mineralogy & Geochemistry, vol. 62, p. 343.

Kaufman, A.A., Keller, G.V., 1981. The Magnetotelluric Sounding Method. Elsevier.

Koukharsky, M., Munizaga, F., Leal, P., Correa, M.J., Brodtkorb, M.K. de, 1999. New K/Ar ages in the Ambargasta and Norte de Córdoba Ranges, Argentina. In: II Simposio Sudamericano de Geología Isotópica, Anales 34. Instituto de Geología y Recursos Minerales, Servicio Geológico Minero Argentino, Villa Carlos Paz, Córdoba, Argentina, pp. 76–77.

Kröhling, D.M., Iriondo, M.H., 2003. El Loess de la Pampa Norte en el Bloque de San Guillermo. AAS Rev. 10 (2), 137–150.

Krystopowicz, N., Currie, C., 2013. Crustal eclogitization and lithosphere delamination in orogens. Earth Planet. Sci. Lett. 361, 195–207.

Leal, P.R., Hartmann, L.A., Santos, J.O.S., Miró, R.C., Ramos, V.A., 2003. Volcanismo postorogénico en el extremo norte de la Sierras Pampeanas Orientales: nuevos datos geocronológicos y sus implicancias tectónicas. Rev. la Asoc. Geol. Argent. 58, 593–607.

Lira, R., Millone, H.A., Kirschbaum, A.M., Moreno, R.S., 1997. Calc-alkaline arc granitoid activity in the Sierra Norte-Ambargasta Ranges, Central Argentina. J. South Am. Earth Sci. 10, 157–177.

Livelybrooks, D., Mareschal, M., Blais, E., Smith, J.T., 1996. Magnetotelluric delineation of the trillabelle massive sulfide body in Sudbury, Ontario. Geophysics 61 (4), 971–986.

Lucero Michaut, H.N., 1979. Sierras Pampeanas del Norte de Córdoba, Sur de Santiago del Estero, Borde Oriental de Catamarca y Angulo Sudeste de Tucumán. In: Segundo Simposio de Geología Regional Argentina, vol. 1. Academia Nacional de Ciencias, Córdoba, pp. 293–347.

Mantovani, M.S.M., Brito Neves, B.B., 2005. The paranapanema lithospheric block: its importance for Proterozoic (Rodinia, Gondwana) supercontinent theories. Gondwana Res. 8 (3), 303–315.

Mareschal, M., Fyfe, W.S., Percival, J., Chan, T., 1992. Grain-boundary graphite in Kapuskasing gneisses and implications for lower-crustal conductivity. Nature 357, 674–676.

Marotta, G.S., França, G.S., Galera Monico, J.F., Fuck, R.A., de Araújo Filho, J.O., 2013. Strain rate of the South American lithospheric plate by SIRGAS-CON geodetic observations. J. South Am. Earth Sci. 47, 136–141.

Martino, R.D., 2003. Las fajas de deformación dúctil de las Sierras Pampeanas de Córdoba: una reseña general. Rev. Asoc. Geol. Argent. 58, 549–571.

McNeice, G.W., Jones, A.G., 2001. Multisite, multifrequency tensor decomposition of magnetotelluric data. Geophysics 66, 158–173.

Millone, H.A., 2004. Ph.D. thesis. Geoquímica y metalogénesis de sistemas hidrotermales con metales base, plata y oro en el basamento neoproterozoico de la Sierra Norte de Córdoba, Argentina, vol. 519. Facultad de Ciencias Exactas, Físicas y Naturales, Universidad Nacional de Córdoba (Unpublished results).

Millone, H.A., Tassinari, C.C.G., Lira, R., Poklepovic, M.F., 2003. Age and strontium–neodymium isotope geochemistry of granitoids of the Sierra Norte-Ambargasta batholith, central Argentina. In: IV South American Symposium on Isotope Geology, Salvador, Bahía, Brasil, Short Papers, vol. II, pp. 617–620.

Miranda, S., Introcaso, A., 1996. Cartas gravimétricas y comportamiento isostático areal de la Sierra de Córdoba, República Argentina. In: XIII Congreso Geológico Argentino y III Congreso de Exploración de Hidrocarburos, vol. 2, pp. 405–417.

Miró, R.C., Gaido, M.F., Candiani, J.C., 1999. Fajas de deformación del batolito Sierra Norte de Córdoba y Santiago del Estero. Actas Congr. Geol. Argent. XIV (I), 152–155.

Miró, R., Saap, M., 2001. Carta Geológica Villa Ojo de Agua, 2963-III, Provincias de Santiago del Estero y Córdoba. scale 1:250,000. Serv. Geol. Minero Argent., Inst. de Geol. Recur. y Miner, Buenos Aires.

Mookherjee, M., Karato, S.-I., 2010. Solubility of water in pyrope-rich garnet at high pressures and temperature. Geophys. Res. Lett. 37, L03310. http://dx.doi.org/10.1029/2009GL041289.

O'Leary, M.S., Lira, R., Dorais, M.J., Tassinarit, C., 2009. Post-collisional lamprophyric event in Sierra Norte, Córdoba, Argentina: mineralogical, geochemical and isotopic characteristics. J. South Am. Earth Sci. 28, 277–287.

Pasotti, P., Castellanos, A., 1963. El relieve de la llanura santafesino-cordobesa comprendida entre los paralelos 32° y 32°30′ S desde 62°45′W hasta el río Paraná, vol. 47. Publicaciones del Instituto de Fisiografía y Geología de la Universidad Nacional de Rosario, pp. 1–79.

Perarnau, M., Gilbert, H., Alvarado, P., Martino, R., Anderson, M., 2012. Crustal structure of the Eastern Sierras Pampeanas of Argentina using high frequency local receiver functions. Tectonophysics 580, 208–217.

Peri, V.G., Pomposiello, C., Favetto, A., Barcelona, H., Rossello, E., 2013. Magnetotelluric evidence of the tectonic boundary between the Río de La Plata Craton and the Pampean terrane (Chaco-Pampean Plain, Argentina): the extension of the transbrasiliano lineament. Tectonophysics 608, 685–699.

Pezzi, E.E., Mozetic, M.E., 1989. Cuencas Sedimentarias de la región Chacoparanaense. In: Chebli, G.A., Spaletti, L.A. (Eds.), Cuencas Sedimentarias Argentinas, Serie Correlación Geológica, vol. 6. INSUGEO, Tucumán, Argentina, pp. 65–78.

Pimentel, M.M., Fuck, R.A., Alvarenga, C.J.S., 1996. Post-Brasiliano (Pan African) high-K granitic magmatism in central Brazil: late Precambrian/early Paleozoic extension. Precambrian Res. 80 (3–4), 217–238.

Ramé, G.A., Miró, R.C., 2011. Modelo geofísico de contacto entre el Orógeno Pampeano y el Cratón del Río de La Plata en las provincias de Córdoba y Santiago del Estero. Ser. Correl. Geol. 27 (2), 111–123.

Ramos, V.A., 1988. Tectonics of the late proterozoic - early paleozoic: a collisional history of southern south America. Episodes 11 (3), 168–174.

Ramos, V.A., Cristallini, E.O., Perez, D.J., 2002. The Pampean flat-slab of the central Andes. J. South Am. Earth Sci. 15, 59–78.

Ramos, V.A., Vujovich, G., Martino, R., Otamendi, J., 2010. Pampia: a large cratonic block missing in the Rodinia supercontinent. J. Geodyn. 50, 243–255.

Ramos, V.A., Martino, R.D., Otamendi, J.E., Escayola, M.P., 2014. Evolución geotectónica de las Sierras Pampeanas Orientales. In: Relatorio del XIX Congreso Geológico Argentino, Córdoba, pp. 965–967.

Rapela, C.W., Bonalumi, A., Baldo, E., 1991. Edad y geoquímica del Pórfido Riolítico de Oncán, Sierra Norte de Córdoba, Sierras Pampeanas, Argentina. Congreso Geológico Chileno, 1991. Resúmenes ampliados, pp. 19–22.

Rapela, C.W., Pankhurst, R.J., Casquet, C., Baldo, E., Saavedra, J., Galindo, C., Fanning, C.M., 1998. The Pampean Orogeny of the southern proto-Andes: Cambrian continental collision in the Sierras de Córdoba. In: Pankhurst, R.J., Rapela, C.W. (Eds.), The Proto-Andean Margin of Gondwana: Geological Society of London, pp. 181–217. Special Publication 142.

Rapela, C.W., Pankhurst, R.J., Casquet, C., Fanning, C.M., Baldo, E.G., González-Casado, J.M., Galindo, C., Dahlquist, J., 2007. The Río de la Plata craton and the assembly of SW Gondwana. Earth-Science Rev. 83 (1–2), 49–82.

Rapela, C.W., Fanning, C.M., Casquet, C., Pankhurst, R.J., Spalletti, L., Poiré, D., Baldo, E.G., 2011. The Rio de la Plata craton and the adjoining Pan-African/brasiliano terranes: their origins and incorporation into south-west Gondwana. Gondwana Res. 20, 673–690.

Richardson, T.J., Gilbert, H.J., Anderson, M.L., Ridgway, K.D., 2012. Seismicity within the actively deforming eastern Sierras Pampeanas, Argentina. Geophys. J. Int. 188, 408–420.

Rodi, W., Mackie, R.L., 2001. Nonlinear conjugate gradients algorithm for 2D magnetotelluric inversion. Geophysics 66 (1), 174–187.

Sabbione, N.C., Rosa, M.L., 2009. Relación VP/VS y espesor cortical en Tornquist (TRQA), Provincia de Buenos Aires, a partir de funciones receptoras (ISBN 978-987-25291-1-6) Actas XXIV Reunión Científica de la AAGG (Sismología): Asociación Argentina de Geofísicos y Geodestas: Ciencias de la Tierra. Buenos Aires, Argentina, pp. 320–326.

Sakaguchi, K., Gilbert, H., Zandt, G., Beck, S., 2003. An investigation into crustal tructure of South America; the continent that is missing some of its Moho (in AGU 2003 fall meeting). (December 2003) EOS. Trans. Am. Geophys. Union 84 (46), 1081.

Santos, T.J.S., Fetter, A.H., Nogueira Neto, J.A., 2008. Comparisons between the northwestern Borborema province, NE Brazil, and the southwestern Pharusian Dahomey Belt, SW Central Africa). In: Pankhurst, R.J., Trouw, R.A.J., Brito Neves, B.B., De Wit, M.J. (Eds.), West Gondwana: Pre-cenozoic Correlations across the Atlantic Region: Geological Society of London Special Publications, vol. 294, pp. 49–67.

Schobbenhaus, C., (coord.), 1975. Carta Geológica do Brasil ao Milionésimo - Folha Goiás (SD 22) (texto explicativo). DNPM, Brasília, 114 pp.

Schwartz, J.J., Gromet, L.P., 2004. Provenance of Late Proterozoic - early Cambrian basin, Sierras de Córdoba, Argentina. Precambrian Res. 129, 1–21.

Schwartz, J.J., Gromet, P.L., Miro, R., 2008. Timing and duration of the calc-alkaline arc of the Pampean orogeny implications for the Late Neoproterozoic to Cambrian evolution of Western Gondwana. J. Geology 116, 39–61.

Selway, K., 2012. Interpreting magnetotelluric data in tectonically stable lithosphere. In: 21st Electromagnetic Induction Workshop, Darwin, Australia,. July 25–31, Review S-5.

Selway, K., Yi, J., Karato, S.-I., 2014. Water content of the Tanzanian lithosphere from magnetotelluric data: implications for cratonic growth and stability. Earth Planet. Sci. Lett. 388, 175–186.

Simpson, C., Law, R.D., Gromet, L.P., Miro, R.C., Northrup, C.J., 2003. Paleozoic deformation in the Sierras de Cordoba and Sierra de Las Minas, eastern Sierras Pampeanas, Argentina. J. South Am. Earth Sci. 15, 749–764.

Simpson, F., Bahr, K., 2005. Practical Magnetotellurics, first ed. University Press, Cambridge.

Sims, J., Ireland, T., Camacho, A., Lyons, P., Pieters, P.E., Skirrow, R., Stuart-Smith, P.G., Miró, R., 1998. U–Pb, Th–PB, and Ar–Ar geochronology from the Southern Sierras Pampeanas, Argentina: implications for the Paleozoic tectonic evolution of the western Gondwana margin. In: Pankhurst, R., Rapela, C.W. (Eds.), The Proto-Andean Margin of Gondwana. Geological Society, London, Special Publications, vol. 142, pp. 259–281.

ten Grotenhuis, S.M., Drury, M.R., Peach, C.J., Spiers, C.J., 2004. Electrical properties of fine-grained olivine: evidence for grain boundary transport. J. Geophys. Res. 109, B06203. http://dx.doi.org/10.1029/2003jb002799.

Tohver, E., Cawood, P.A., Rossello, E.A., Jourdan, F., 2012. Closure of the Clymene Ocean and formation of West Gondwana in the Cambrian: evidence from the Sierras Australes of the southernmost Rio de la Plata craton, Argentina. Gondwana Res. 21 (2–3), 193–222.

Trindade, R.I.F., D'Agrella-Filho, M.S., Epof, I., Brito-Neves, B.B., 2006. Paleomagnetism of Early Cambrian Itabaiana mafic dikes (NE Brazil) and the final assembly of Gondwana. Earth Planet. Sci. Lett. 244 (1–2), 361–377.

Trompette, R., 1994. Geology of Western Gondwana, Pan-African - Brasiliano Aggregation of South America and Africa. A. A. Balkema, Rotterdam, Brookfield, 350 pp.

Türkoğlu, E., Unsworth, M., Çağlar, I., Tuncer, V., Avşar, Ü., 2008. Lithospheric structure of the Arabia-Eurasia collision zone in eastern Anatolia: magnetotelluric evidence for widespread weakening by fluids? Geology 36, 619–622.

von Gosen, W., Prozzi, C., 2010. Pampean Deformation in the Sierra Norte de Córdoba, Argentina: Implications for the collisional history at the Western pre-Andean Gondwana margin: Tectonics, vol. 29, p. TC2012. http://dx.doi.org/10.1029/2009TC002580.

Vozzoff, K., 1972. The magnetotelluric method in the exploration of sedimental basins. Geophysics 37 (1).

Wannamaker, P.E., Hasterok, D.P., Johnston, J.M., Stodt, J.A., Hall, D.B., Sodergren, T.L., Pellerin, L., Maris, V., Doerner, W.M., Groenewold, K.A., Unsworth, M.J., 2008. Lithospheric dismemberment and magmatic processes of the Great Basin-Colorado plateau transition, Utah, implied from magnetotellurics. Geochem. Geophys. Geosystems 9, 1–38.

Wiens, F., 1985. Phanerozoic tectonics and sedimentation in the Chaco Basin of Paraguay, with comments on hydrocarbon potential. In: Tankard, A.J., Suarez Soruco, R., Welsink, H.J. (Eds.), Petroleum Basins in South America, vol. 62. AAPG Memoir, pp. 185–205.

Yang, X., Keppler, H., McCammon, C., Ni, H., Xia, Q., Fan, Q., 2011. Effect of water on the electrical conductivity of lower crustal clinopyroxene. J. Geophys. Res. Solid Earth 116, B04208. http://dx.doi.org/10.1029/2010jb008010.

Yang, X., Keppler, H., McCammon, C., Ni, H., 2012. Electrical conductivity of orthopyroxene and plagioclase in the lower crust. Contrib. Mineral. Petrol. 163 (1), 33–48.

Yoshino, T., Nishi, M., Matsuzaki, T., Yamazaki, D., Katsura, T., 2008. Electrical conductivity of majorite garnet and its implications for electrical structure in the mantle transition zone. Phys. Earth Planet. Inter. 170 (3–4), 193–200.

Yoshino, T., Matsuzaki, T., Shatskiy, A., Katsura, T., 2009. The effect of water on the electrical conductivity of olivine aggregates and its implications for the electrical structure of the upper mantle. Earth Planet. Sci. Lett. 288 (1–2), 291–300.

Zanor, G., Piovano, E.L., Ariztegui, D., Vallet-Coulomb, C., 2012. A modern subtropical playa complex: Salina de Ambargasta, central Argentina. J. South Am. Earth Sci. 35, 10–26.